Supercrystals of CdSe Quantum Dots with High Charge Mobility and Efficient Electron Transfer to TiO_2

Elise Talgorn,[†] Ruben D. Abellon,[†] Patricia J. Kooyman,[‡] Jorge Piris,[†] Tom J. Savenije,[†] Albert Goossens,[†] Arjan J. Houtepen,[†,*] and Laurens D. A. Siebbeles[†,*]

[†]Optoelectronic Materials Section and [‡]Catalysis Engineering Section, Department of Chemical Engineering, Delft University of Technology, Julianalaan 136, 2628 BL Delft, The Netherlands

ABSTRACT Thermal annealing of thin films of CdSe/CdS core/shell quantum dots induces superordering of the nanocrystals and a significant reduction of the interparticle spacing. This results in a drastic enhancement of the quantum yield for charge carrier photogeneration and the charge carrier mobility. The mobile electrons have a mobility as high as 0.1 $cm^2/(V \cdot s)$, which represents an increase of 4 orders of magnitude over non-annealed QD films and exceeds existing literature data on the electron mobility in CdSe quantum dot films. The lifetime of mobile electrons is longer than that of the exciton. A fraction of the mobile electrons gets trapped at levels below the conduction band of the CdSe nanocrystals. These electrons slowly diffuse over 50−300 nm on longer times up to 20 μs and undergo transfer to a TiO_2 substrate. The yield for electron injection in TiO_2 from both mobile and trapped electrons is found to be >16%.

KEYWORDS: quantum dot · annealing · supercrystal · photoconductivity · TiO_2

In the past decade, semiconductor quantum dots (QDs) have emerged as promising new building blocks for optoelectronic devices.[1,2] In particular, photovoltaic applications have received a vast amount of attention.[3,4] Tuning of the energy of the electronic levels is possible by controlling the QD size and type, allowing great flexibility in solar cell design. One of the potential applications is to build multi-gap systems which are better matched to the solar spectrum than single-gap systems.[5] Furthermore, multiexciton generation has been reported to occur in QDs,[6−9] which could increase the efficiency of solar cells if the multiexcitons can dissociate into free charges.[10]

QDs can be prepared in a cheap and simple manner using colloidal chemistry. With this method, QDs of many different compositions can be obtained with a high luminescence quantum yield and a narrow size distribution.[11,12] The surface of QDs in solution is usually terminated by organic surfactants, which prevent QD aggregation and passivate surface states. For device applications, the QDs are deposited in the form of a thin film. The performance of optoelectronic devices depends to a large extent on the mobility of charge carriers through the QD film. Unfortunately, the commonly used bulky organic surfactants that passivate the QD surface act as a barrier for charge transport between the QDs. Indeed, replacement of bulky surfactants by small capping molecules in PbSe QD films has resulted in a dc charge carrier mobility of 1 $cm^2/(V \cdot s)$.[13] For films of CdSe QDs with small surface ligands, the highest electron mobilities reported to date are on the order of 10^{-2} $cm^2/(V \cdot s)$.[14−17]

The electronic coupling between QDs, and consequently the charge carrier mobility, can be enhanced by removing the organic surfactants from the QD surface. Removal of surfactants from a film of CdSe QDs has been realized by thermal annealing and was found to result in reduction of the interparticle distance or sintering of the QDs, depending on the conditions.[18,19] Surface defects resulting from removal of capping molecules can be passivated by growing a thin shell of a high band gap inorganic material around the core. Indeed, introduction of a ZnS shell around CdSe QDs has demonstrated the importance of reduction of surface states on the photoconductivity of QD films.[20] CdS is an alternative shell material of interest because the band offset between the LUMO of CdSe and CdS is small, allowing the electron wave function to delocalize over the shell, while the hole wave function is localized in the core, reducing hole trapping at surface sites.[21]

The aim of the present work is to enhance the photoconductance of films of CdSe/CdS core/shell QDs by removing the surfactant molecules *via* thermal annealing.

*Address correspondence to a.j.houtepen@tudelft.nl, l.d.a.siebbeles@tudelft.nl.

Received for review November 26, 2009 and accepted February 11, 2010.

Published online February 25, 2010. 10.1021/nn901709a

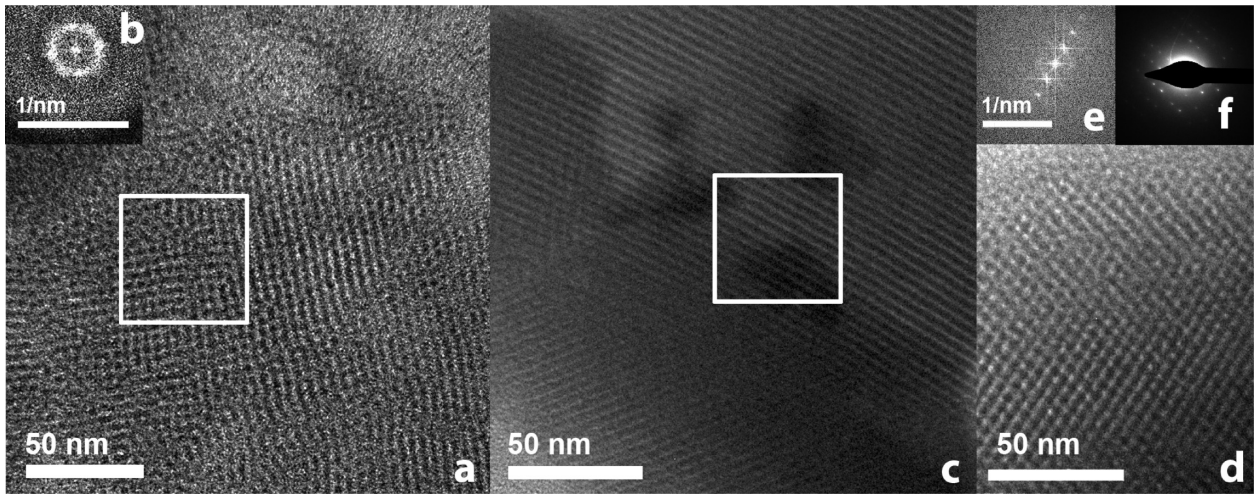

Figure 1. TEM images of QD films before (a) and after (c,d) thermal annealing. The images in c and d show supercrystals under different projections. Insets: fast Fourier transforms of the domains indicated by the square, before (b) and after (e) thermal annealing. For the thermally annealed sample, the wide-angle electron diffraction pattern is also shown (f).

Structural analysis using optical techniques and electron microscopy demonstrates that moderate thermal annealing conditions result in efficient removal of organic ligands and a concomitant shortening of the interparticle distance. Moreover, a marked increase of the long-range order in the QD arrays is observed. The photoconductance was measured with the time-resolved microwave conductivity technique (TRMC).[22] The great advantage of this technique is that the intrinsic photoconductance of the system can be measured without the need to use contacting electrodes. The TRMC technique provides information about both the polarizability of neutral excitons and the mobility of excess charge carriers. It is found that thermal annealing of the QD film significantly enhances the photogeneration yield and the mobility of charge carriers. The mobility of the charge carriers decays on a time scale of tens of nanoseconds. Studies of the dynamics of electron transfer to a TiO_2 layer on longer time scales show that relaxed electrons can undergo diffusion over distances of 50−300 nm, followed by efficient transfer to the TiO_2.

RESULTS AND DISCUSSION

Effect of Thermal Annealing on the Structural and Optical Properties of the QD Film. Figure 1 shows transmission electron microscopy (TEM) images of a CdSe/CdS core/shell QD film on a silicon nitride grid before and after thermal annealing. The non-annealed film is composed of a dense array of QDs with short-range ordering. The QD diameter determined from the TEM image is 3.1 nm with a size dispersion of ~5%. The interparticle distance can be determined from a fast Fourier transform (FFT) of the TEM image. Such a FFT shows a clear ring in reciprocal space (Figure 1b), which means that neighboring QDs have a well-defined interparticle distance. By averaging the values calculated for different areas in the QD film, an average edge-to-edge interparticle distance of 1.4 ± 0.3 nm is obtained. This is close to the expected length for the capping molecules tri-*n*-octylphosphine oxide (TOPO), hexadecylamine (HDA), and *n*-tetradecylphosphonic acid (TDPA). The infrared transmission spectrum of such a non-annealed QD film (Figure 2, solid line) clearly exhibits features due to C−H stretching vibrations in the alkyl chains of the capping molecules between 2800 and 3000 cm^{-1}, as well as transitions involving N−H stretching vibrations in HDA around 3200 cm^{-1}.

Aiming to reduce the interparticle distance, the QD film was thermally annealed for 1 h at 190 °C at 1 mbar pressure. In the infrared transmission spectrum (Figure 2, dotted line), the features corresponding to the C−H stretching vibrations are strongly reduced and those due to the N−H stretching vibrations disappear completely. This demonstrates that most of the organic surfactant has been removed from the QD surface by thermal annealing. The TEM image in Figure 1c,d shows

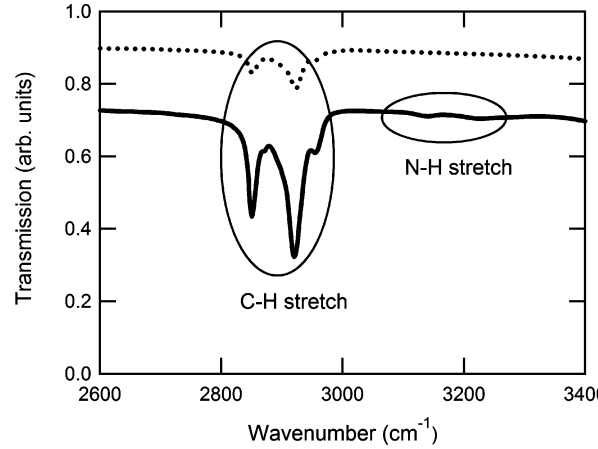

Figure 2. IR transmission spectra of the QD film on quartz before (solid line) and after (dotted line) thermal annealing. Note that an offset between the spectra has been introduced to facilitate distinction of the curves.

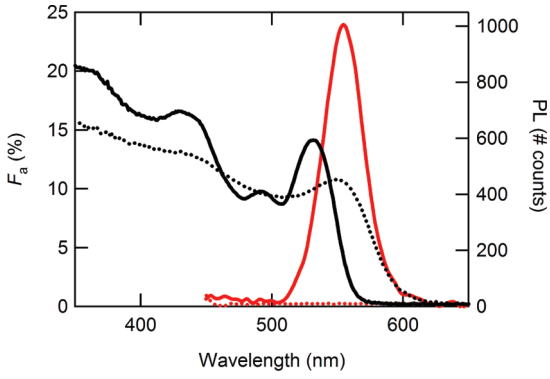

Figure 3. Attenuation spectra (black lines) and photoluminescence spectra (red lines) of the QD film on quartz before (solid lines) and after (dotted lines) thermal annealing.

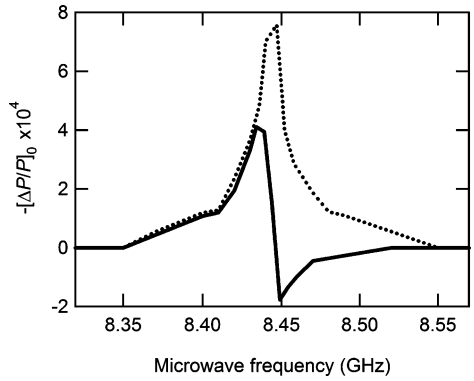

Figure 4. Maximum of the relative change in microwave power as a function of microwave frequency for a QD film on quartz before (solid line) and after (dotted line) thermal annealing. The pump wavelength corresponds to the first absorption peak of the samples. The average number of absorbed photons per QD is 0.3 for the non-annealed film and 0.003 for the annealed film.

that highly ordered QD domains are formed. These domains, also called supercrystals, present a regular packing of QDs over hundreds of nanometers. No growth or sintering of the QDs is observed. A FFT of a supercrystal area is depicted in Figure 1e and shows a line of sharp spots, which reflects the very regular packing of the QDs. From several FFTs and taking into account the projections under which the supercrystals are imaged, the average edge-to-edge interparticle distance is calculated to be 0.7 $\pm$ 0.1 nm, which is half of the edge-to-edge distance before thermal annealing. The interparticle distance is reduced due to partial removal of surfactant molecules. Figure 1f shows a wide-angle electron diffraction pattern (WAED) of the supercrystal shown in Figure 1c. A WAED pattern is sensitive to the crystalline structure within the QDs. The WAED pattern of Figure 1f consists of sharp spots, indicating that the atomic lattices of the individual QDs are aligned within the supercrystal.

It must be realized that thermal annealing can also lead to sintering of the QDs in a film. As discussed above, TEM images of QD films on a silicon grid show no sign of sintering (see Figure 1c,d). However, the morphology of these films may differ from that of a QD film on a quartz substrate, as used for the photoconductance measurements. To obtain more direct information about the structure of the actual films that were used for photoconductance studies, scanning electron microscopy (SEM) measurements with a resolution of 5 nm were carried out. The SEM images did not show any sintering of QDs either.

The optical absorption spectrum of the non-annealed QD film in Figure 3 exhibits well-resolved features with a first absorption peak at 534 nm, which corresponds to QDs with a diameter of 2.7−2.8 nm,[23,24] close to the size determined from the TEM images (the diameter obtained from TEM is 3−4 Å larger, which corresponds to the CdS shell). Thermal annealing causes absorption features to broaden and the first absorption peak to shift to 553 nm. The absorption spectrum after thermal treatment clearly corresponds to CdSe NCs of less than 4 nm,[23,24] indicating that the film is still composed of quantum-confined particles. The broadening and red shift are attributed to an increase of the electronic coupling between the QDs, as a result of the reduction of the interparticle distance.[25] The photoluminescence spectrum consists of a single sharp peak, which is completely quenched after thermal annealing. The increased electronic coupling between QDs in the thermally annealed film will facilitate exciton delocalization and motion through the QD film, which enhances the probability to encounter a defect site or surface state, where quenching occurs. In addition, the removal of most of the organic surfactants will likely increase the number of such surface states. Also, stronger electronic coupling can lead to a weaker Coulomb interaction between the photoexcited electron and the hole, which will enhance the yield of charge carriers. Nonradiative recombination of charges then results in quenching of the photoluminescence.

In summary, thermal annealing of CdSe/CdS core/shell QD films leads to the removal of a significant part of the organic capping molecules and the formation of a film with long-range order, including even crystallographic alignment, with an interparticle distance of 0.7 nm. No sintering or growth of the QDs was observed. Thermal annealing causes complete quenching of photoluminescence and a red shift and broadening of the optical absorption, which is attributed to enhanced electronic coupling between the QDs.

Effect of Thermal Annealing on the Photoconductance of the QD Film. Photogeneration and mobility of charge carriers in the QD films were investigated with the time-resolved microwave conductivity (TRMC) technique.[22,26] Figure 4 shows the relative change in microwave power reflected from the microwave cavity upon photoexcitation of QD films at the first absorption peak of the QDs. To achieve a satisfactory signal-to-noise ratio for the non-annealed film, a high pump fluence was needed, leading to an average of 0.3 absorbed photons per QD, as calculated by assuming a homogeneous absorption

throughout the depth of the film and using the extinction coefficient for CdSe QDs from ref 27. The relative change in microwave power has opposite sign on different sides of the resonance frequency (8.444 GHz), which implies that the photoconductance has a significant imaginary component (see Figure 9). The imaginary photoconductance of the non-annealed QD film is attributed to photogeneration of excitons. The asymmetry in the frequency dependence of the relative change in microwave power is due to the presence of a small real component of the photoconductance. The product of the quantum yield for photogeneration of charge carriers, Φ_0, and the sum of the mobility of electrons and holes, $\Sigma\mu$, determined from the real photoconductance is $\Phi_0\Sigma\mu = 2 \times 10^{-5}$ cm^2/(V · s). The fact that the imaginary component, which is due to excitons, strongly dominates over the real component (free charge carriers) is qualitative evidence for a very low yield of charge carrier formation. Such a low yield can be explained by the high exciton binding energy of several tens of an electronvolt[28] and the presence of bulky surface molecules that lead to a large interparticle spacing, which is unfavorable for electronic coupling and delocalization of the excited electron over different QDs. The small electronic coupling will also lead to a low charge carrier mobility. Ginger *et al.* estimated an electron mobility of 10^{-6}–10^{-4} cm^2/(V · s) in films of TOPO-capped CdSe QDs.[29]

As shown in Figure 4, the relative change in microwave power of the thermally annealed QD film is positive and symmetrical around the resonance frequency. This means that the photoconductance is predominantly real, while the imaginary conductance is negligible. Hence, thermal annealing leads to an increase of the quantum yield of charge carrier formation and/or the charge mobility.

In what follows, the real component of the photoconductance as obtained from measurements at the resonance frequency of the microwave cavity will be considered. The real component of the photoconductance is likely due to mobile electrons rather than holes since the hole is confined to the CdSe core and does hardly penetrate into the CdS shell.[21]

The effect of the initial density of photoexcitations in the QD film on the photoconductance was investigated by variation of the pump laser fluence. Figure 5 shows the photoconductance normalized to the incident pump laser fluence. The initial rise of the transient is determined by the 18 ns response time of the microwave cavity. When the average number of photoexcitations exceeds 0.01 per QD, the magnitude of the incident-fluence-normalized photoconductance, $\Delta G_0/I_0$, decreases and the decay becomes faster. This indicates that second-order decay processes, such as bimolecular exciton annihilation (at short times) or charge recombination, are important if on average more than 0.01 excitons are generated per QD. Hence, as a result of

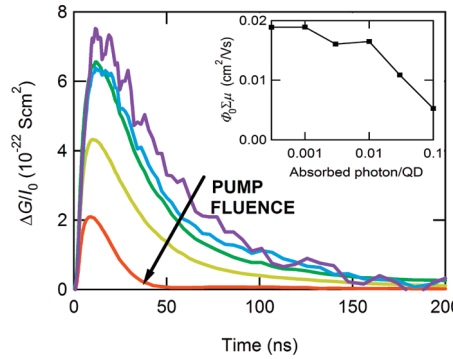

Figure 5. Incident-fluence-normalized photoconductance transients for a thermally annealed QD film on quartz. The pump fluence corresponds to 0.001 (purple), 0.003 (blue), 0.01 (green), 0.03 (yellow), and 0.1 (orange) absorbed photons per QD. Inset: $\Phi_0\Sigma\mu$ as a function of the average number of absorbed photons per QD.

the increased exciton and charge mobility, excitons and/or charge carriers encounter at least 100 QDs within 18 ns. After deconvolution with the instrumental response, the decay of the charges at low fluence, where the second-order processes are negligible, can be fitted as a double exponential decay with lifetimes of 12 and 200 ns. It is noticeable that the lifetime of mobile charge carriers is longer than the exciton radiative lifetime of 17 ns.[30]

Unless stated otherwise, all of the following measurements were done in the low pump fluence limit.

The inset of Figure 5 illustrates that $\Phi_0\Sigma\mu$ is almost constant in the lowest fluence range with a value approaching 0.02 cm^2/(V · s). It must be noted that the sample-to-sample variations were significant with $\Phi_0\Sigma\mu$ between 0.005 and 0.1 cm^2/(V · s), which is likely due to subtle differences in the drying process of the drop-casted films. The results in Figure 5 were obtained for a representative QD film with $\Phi_0\Sigma\mu$ in the middle of the range of measured values. The average $\Phi_0\Sigma\mu$ over five prepared films is 0.03 cm^2/(V · s). Hence, thermal annealing enhances $\Phi_0\Sigma\mu$ by about 3 orders of magnitude. The values obtained for $\Phi_0\Sigma\mu$ are comparable to the highest electron mobility reported in the literature for CdSe QD films (0.01 cm^2/(V · s) at high doping densities[14,15] and 0.03 cm^2/(V · s) for metal chalcogenide capped QDs[16]). It is of interest to note that, in case the microwave mobility is comparable to these mobility values from the literature, the initial quantum yield for charge carrier photogeneration would be close to 100%. For the case of a much smaller quantum yield, the microwave mobility largely exceeds literature data.

As mentioned above, the photoconductance is likely due to mobile electrons rather than holes.[21] Electron motion from one QD to another can be considered as a process of tunneling through the energy barrier between the QDs.[31,32] The electron transfer rate can then be expressed as $\Gamma = \Gamma_0 \exp[-(2m^*\Delta E/\hbar^2)^{1/2}\Delta x]$, where Γ_0 is the rate at vanishing barrier height or width, m^* is the effective mass of the charge carrier, ΔE is the bar-

rier height, and Δx its width.[33] The ratio of the charge mobilities for annealed and non-annealed QD films is then

$$\frac{\mu_{annealed}}{\mu_{non\text{-}annealed}} = \frac{\exp[-(2m^*\Delta E_{annealed}/\hbar^2)^{1/2}\Delta x_{annealed}]}{\exp[-(2m^*\Delta E_{non\text{-}annealed}/\hbar^2)^{1/2}\Delta x_{non\text{-}annealed}]} \frac{d_{annealed}^2}{d_{non\text{-}annealed}^2} \quad (1)$$

In eq 1, the distances $d_{non\text{-}annealed}$ and $d_{annealed}$ refer to the distance between the center of adjacent QDs. The barrier width corresponds to the interparticle distance, which was determined from TEM measurements. Due to the small electron affinity and small density-of-states of the organic surfactants, the barrier for electron tunneling between QDs, ΔE, can to a good approximation be taken equal to the electron affinity of CdSe QDs, which is about 4 eV.[34,35] Taking the effective mass of electrons equal to the CdSe bulk value of 0.13 m_0,[36] eq 1 gives $\mu_{annealed}/\mu_{non\text{-}annealed} = 10$. According to this result, the increase of $\Phi_0\Sigma\mu$ by 3 orders of magnitude as a consequence of reduction of the interparticle distance cannot be solely due to enhancement of the charge mobility. This suggests that thermal annealing causes the quantum yield, Φ_0, to increase by about 2 orders of magnitude. Thermal annealing induces a reduction of the interparticle distance, which can enhance delocalization of the wave function of an excited electron over different QDs. Electron delocalization then reduces the electron−hole wave function spatial overlap as well as the electron−hole Coulomb interaction, which results in a higher probability for free charge formation. According to the above details, reduction of the interparticle distance induces a concomitant increase of charge carrier mobility and free charge formation yield. The electron diffraction pattern shown in Figure 1f indicates that the atomic lattices of the quantum dots within a supercrystal are aligned. Since the QD facets are crystallographically determined, they are consequently also aligned. This may enhance the local coupling between QDs and may in part be responsible for the high photoconductivity.

The effect of the pump wavelength on the incident-fluence-normalized photoconductance is depicted in Figure 6. The photoconductance spectrum resembles the optical attenuation spectrum, proving that the measured photoconductivity is due to mobile charges created *via* absorption of light by the QDs. The contribution of larger aggregates to the photoconductivity can be excluded since the absorption exhibits a first exciton peak typical for QDs. Interestingly, the normalized photoconductance diverges from the optical attenuation, F_a, at shorter wavelengths. This must be due to an increase of the quantum yield for charge carrier photogeneration with photon energy. For higher energy, the excited electron likely exhibits a larger degree of

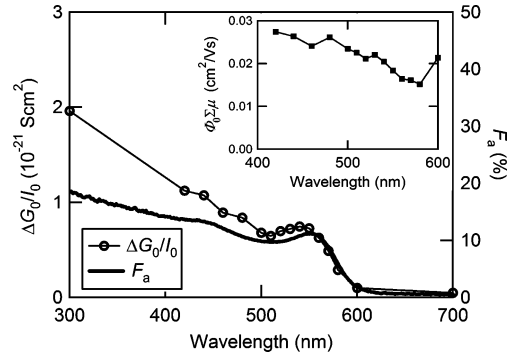

Figure 6. Maximum of the incident-fluence-normalized photoconductance as a function of pump wavelength (left axis, open circles) and optical attenuation spectrum (right axis, solid line) for a thermally annealed QD film on quartz. The pump fluence corresponds to an average of 0.003 absorbed photons per QD. Inset: $\Phi_0\Sigma\mu$ as a function of wavelength.

delocalization over different QDs, which enhances the probability for formation of free electrons and holes.[37]

In order to study the effect of the CdS shell on the photoconductance, films of CdSe QDs without a shell were also studied. The photoconductance of thermally annealed CdSe QD films was found to be negligible as compared with that for films of CdSe/CdS core/shell QDs. The small photoconductance for CdSe QD films is possibly due to decay of charges at unpassivated surface states. This is in accordance with the work of Porter *et al.*, which stresses the importance of an inorganic shell to passivate surface defect states in order to obtain a high photoconductivity in QD films.[20]

In summary, it was found that thermal annealing increases the photoconductance of CdSe/CdS core/shell QD film by 3 orders of magnitude, which is due to an increase in both charge mobility and quantum yield for charge carrier photogeneration. The photoconductance of films of CdSe QDs without a CdS shell is much smaller than in the presence of a shell. This is likely due to charge trapping at unpassivated surface states.

Electron Transfer from CdSe/CdS Core/Shell QDs to TiO_2. The effect of thermal annealing on photoinduced electron transfer from the QDs to TiO_2 was studied by drop-casting a QD film on a layer of smooth TiO_2. The latter material was chosen as an electron-accepting substrate because of its high electron affinity[38] and the long electron lifetime before trapping or recombination,[39,40] allowing easy detection of the injected conduction electrons. The large band gap of TiO_2 (3.2 eV) permits selective photoexcitation of the QDs, while the high ionization potential of TiO_2 makes hole injection energetically impossible.[41]

Figure 7 shows the time-dependent photoconductance obtained by excitation of the QDs at the maximum of the first absorption peak. The photoconductance of the non-annealed QD/TiO_2 bilayer is negligible. This shows that the bulky surfactant molecules prevent exciton or electron motion from the QD layer to the interface with TiO_2. However, after thermal anneal-

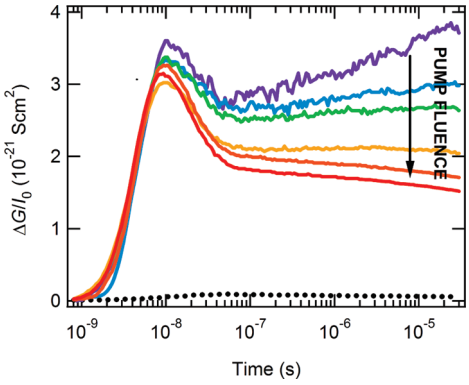

Figure 7. Incident-fluence-normalized photoconductance transients for a QD film on TiO_2 before (black dotted curve) and after (colored solid curves) thermal annealing. The pump wavelength corresponds to the first absorption peak of the QDs. For the annealed sample, the pump laser fluence was varied from 0.0003 to 0.02 absorbed photons per QD.

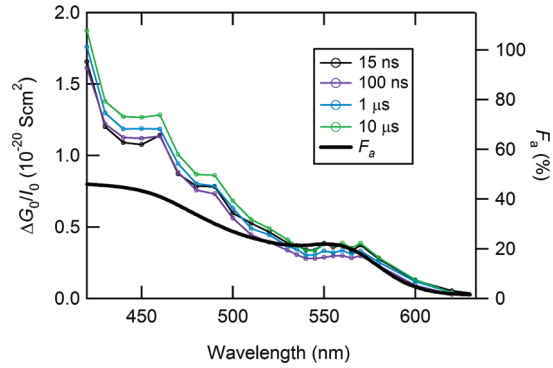

Figure 8. Maximum of the incident-fluence-normalized photoconductance (left axis, symbols) at different times after the laser pulse and optical attenuation spectrum (right axis, drawn curve) for a thermally annealed QD/TiO_2 bilayer. The pump fluence leads to 0.0003 absorbed photons per QD.

ing, a significant long-lived photoconductance is observed (see Figure 7). While the photoconductance of a QD film on quartz has completely decayed within ~200 ns (see Figure 5), the photoconductance of the QD/TiO_2 bilayer persists for at least 20 μs (see Figure 7). At times shorter than 100 ns, the photoconductivity of the QD/TiO_2 bilayer exhibits a decay that is similar to that for the QD film on quartz in Figure 5. Apparently, at these times, a significant fraction of the charges undergoes decay by relaxation of the mobility (*i.e.*, the charges migrate to the largest QDs which act as shallow traps in the ensemble) or by recombination within the QD layer. The photoconductance of the QD/TiO_2 bilayer at times longer than ~200 ns must be due to electrons in TiO_2 because, at these times, the photoconductance of a QD film on quartz has decayed (see Figure 5). Mobile electrons and possibly excitons can diffuse to the interface between the QD layer and the TiO_2 layer, where electron transfer to TiO_2 can occur. This gives rise to a long-lived photoconductance since back recombination of electrons in TiO_2 with holes in the QD layer is expected to take place on a time scale longer than 100 μs.[40] For low pump laser fluence, the photoconductance of the QD/TiO_2 bilayer rises during at least 20 μs (see Figure 7). This rise is due to slow electron diffusion from the QDs to TiO_2. These slowly diffusing electrons may be trapped at levels below the conduction band of CdSe nanocrystals[35,42,43] and have negligible contribution to the photoconductance of a QD layer on quartz. For higher pump fluence, the photoconductance exhibits a slight decay on longer times. This decay can be attributed to second-order interfacial recombination of holes in the QD layer and electrons in the TiO_2 layer.

Figure 8 shows the wavelength dependence of the normalized photoconductance at different times after the laser pulse. For all times, the normalized photoconductance response follows the optical attenuation, with a deviation at lower wavelength. This is similar to what has been found for the QD film on quartz (Figure 6) and proves that, at all times, the photoconductance results from charges or excitons initially generated in the QDs.

The incident photon to charge separation efficiency (IPCSE) was obtained by comparing the photoconductance of the QD/TiO_2 bilayer to that of a bare TiO_2 layer, according to

$$\mathrm{IPCSE}(\lambda) = \frac{[\Phi_0\Sigma\mu]_\lambda}{[\Phi_0\Sigma\mu]_{300\mathrm{nm}}}\frac{1}{(F_a)_\lambda} \qquad (2)$$

In eq 2 the factor $[\Phi_0\Sigma\mu]_{300\mathrm{nm}}$ was obtained from the photoconductance of a bare TiO_2 layer photoexcited at 300 nm. This factor corresponds to the electron mobility in TiO_2 because Φ_0 can be taken as 100% and the hole mobility is negligible.[44] For bare TiO_2 functionalized with MPA and submitted to thermal annealing, $[\Phi_0\Sigma\mu]_{300\mathrm{nm}}$ was measured to be 1.7 $cm^2/(V \cdot s)$. For QD films with thicknesses between 300 and 1000 nm, the IPSCE at 20 μs after the pump pulse was 1.51 ± 0.03%, for a pump fluence leading to 0.0003 absorbed photons per QD. It was not possible to obtain homogeneous films with a thickness below 300 nm. The fact that the IPCSE is constant for films thicker than 300 nm implies that the *active layer* (the diffusion length of the electrons or excitons in the QD film that contribute to electron injection into TiO_2) is thinner than 300 nm. The lower limit to the thickness of the active layer is obtained by assuming Φ_0 = 100% and determining the thickness for which the fraction of absorbed photons is equal to the IPCSE. Using the optical extinction coefficient of CdSe QDs from ref 27, the lower limit to the active layer thickness is 50 ± 10 nm. Hence, the active layer thickness is 50−300 nm, and the charge separation efficiency per absorbed photon within the active layer is 16−100%.

CONCLUSIONS

Thermal annealing of CdSe/CdS core/shell QD films leads to removal of the organic surfactants and formation of a highly ordered array of QDs with interparticle

separation of only 0.7 nm. No sintering or growth of the nanocrystals is observed. Annealing causes a red shift and a broadening of the optical absorption, which is attributed to enhanced electronic coupling between the QDs.

Photoexcitation of a non-annealed film of QDs with bulky surfactant molecules leads predominantly to formation of excitons, which are confined to the individual QDs. After thermal annealing, the photoconductivity of the QD films is improved by more than 3 orders of magnitude due to an enhanced quantum yield for charge generation and a higher charge carrier mobility. The lower limit to the charge mobility is as high as 0.005−0.1 $cm^2/(V \cdot s)$, with the range determined by sample-to-sample variations. The high mobility results from the short interparticle separation and high degree of order in the supercrystals. The presence of a CdS shell was necessary to achieve a high photoconductivity, which indicates the importance of passivation of surface traps.

Transfer of relaxed electrons with a low mobility from a thermally annealed QD layer to a smooth TiO_2 substrate was found to occur on a time scale of at least 20 μs. During this time, the electrons undergo slow diffusion over a distance of 50−300 nm.

METHODS

QD Synthesis and Film Preparation. CdSe QDs were synthesized under N_2 atmosphere following the "green" recipe of Mekis *et al.*[46] This synthesis results in QDs stabilized by tri-*n*-octylphosphine oxide (TOPO), hexadecylamine (HDA), and *n*-tetradecylphosphonic acid (TDPA) surfactant molecules. The synthesis was carried out using anhydrous solvents. The QDs were precipitated with methanol, filtered, and redispersed in toluene. To remove free surfactant molecules from the solvent, this procedure was repeated three times, and the QDs were finally dispersed in toluene. A CdS shell was grown around the CdSe cores following the procedure described in ref 45; however, cadmium diacetate was used instead of dimethylcadmium. The QDs were purified as described above and redispersed in a 9:1 v/v hexane/octane mixture. From the amount of reactants used for the CdS shell growth, and using the lattice parameter of wurtzite CdS, it can be estimated that the shell consists of 1.5 monolayers of CdS. The shell growth resulted in a marked increase of the photoluminescence quantum yield, confirming full coverage of the CdSe core.[21]

CdS-capped CdSe QD films were deposited on quartz substrates or 100 nm thick anatase TiO_2 on quartz substrates (Everest Coating, Delft, The Netherlands). The TiO_2 films (without the QDs) were annealed for 2 h at 450 °C in air. To efficiently bind the QDs to the substrates, the TiO_2 films or the quartz plates were dipped into a solution of 1 M mercaptopropionic acid (MPA) and 0.1 M H_2SO_4 in acetonitrile for 4 h.[46] MPA acts as a linker that covalently attaches to the quartz or TiO_2 surface on one side and to the QDs on the other side. The substrates were rinsed with acetonitrile and toluene and dipped overnight in a solution of QDs to ensure binding of the QDs to the TiO_2 *via* the MPA molecule. Subsequently, the QD solutions were drop-casted on the substrates, and the samples were covered in order to induce slow drying. This procedure results in films with a typical thickness of 400 nm and a typical surface roughness of 60 nm, as determined with a Veeco Dektak 8 step-profilometer. Finally, the films were vacuum-annealed (at 1 mbar pressure with air as the residual gas) for 1 h at 190 °C. Bare TiO_2 functionalized with MPA was subjected to an identical thermal annealing in order to be used as a reference for photoconductivity measurements.

Structural and Optical Characterization. The QD films were characterized by transmission electron microscopy (TEM) using a FEI Tecnai TF20 electron microscope with a field emission gun as the source of electrons operated at 200 kV. Samples were mounted on DuraSiN silicon nitride supported by a silicon grid by placing a few droplets of the QD suspension on the grid, followed by drying at ambient conditions. For imaging the effect of thermal annealing, the grids were then annealed under conditions identical to the studied samples. A FEI Quanta 200F scanning electron microscope (SEM) was used to characterize the surface of the QD films on quartz. Imaging was performed with primary and secondary electrons at various energy and angles in low vacuum to prevent charging of the sample.

Infrared transmission spectra were recorded on a Thermo Nicolet Fourier transform infrared (FTIR) spectrometer. Spectra were measured in the 2100−6000 cm^{-1} spectral range with a resolution of 4 cm^{-1} by averaging 100 individual spectra. The spectra were corrected for absorption of the quartz substrate.

Optical absorption spectra were measured using a Perkin-Elmer Lambda 900 spectrometer equipped with an integrating sphere. The fraction of transmitted (F_t) and reflected (F_r) photons was measured, and the fraction of photons absorbed (F_a), called attenuation, was calculated as $F_a = 1 - F_t - F_r$.

A Lifespec-ps setup using a 405 nm excitation source (Edinburgh instrument) was used for photoluminescence measurements.

Time-Resolved Microwave Conductivity Technique. The photoconductance of QD films was measured using the time-resolved microwave conductivity (TRMC) technique. The TRMC setup has been described in detail previously.[22,26] The samples were mounted in an X-band microwave cavity at a position of maximum electric field (100 V/cm). Upon photoexcitation, the change in microwave power reflected from the cavity was measured. Photoexcitation laser pulses of 3 ns duration with a wavelength in the range of 420−700 nm range were obtained by pumping an optical parametric oscillator with the third harmonic of a Q-switched Nd:YAG laser. Pulses with a wavelength of 300 nm were produced by frequency-doubling the 600 nm pulse. The photon flux was varied between 10^{13} and 2×10^{15} photons/cm^2/pulse, using neutral density filters.

The change in reflected microwave power can be due to a change in the real and/or the imaginary component of the conductance of the sample.[47] Mobile charges that move with a velocity in phase with the oscillating microwave field give rise to a real conductance component, which leads to absorption of microwave power. In the case of pure real conductance, the microwave power reflected from the cavity is reduced for all microwave frequencies, with the reduction being maximal at the resonance frequency of the cavity, as depicted in Figure 9a. The polarizability of excitons leads to a change of the imaginary conductance and causes a phase shift of the microwaves. A pure imaginary conductance results in a shift of the resonance frequency of the cavity, as illustrated in Figure 9a. Figure 9b shows the corresponding relative changes in microwave power due to photoexcitation of the sample, defined as $-\Delta P(t)/P = (P_{dark} - P_{light}(t))/P_{dark}$ with t the time, P_{light} the reflected microwave power after laser excitation of the sample, and P_{dark} the reflected power without laser excitation. For a pure real photoconductance $-\Delta P(t)/P$ is positive at all microwave frequencies, as exemplified in Figure 9b. For a purely imaginary photoconductance, the shift of the resonance frequency of the microwave cavity causes $-\Delta P(t)/P$ to be positive at lower frequency and negative at higher frequencies.

For small photoinduced changes in the real conductance, $\Delta G(t)$, of the sample and negligible change in imaginary conductance, the relative change in microwave power is

$$\frac{\Delta P(t)}{P} = -K\Delta G(t) \qquad (3)$$

The sensitivity factor K in eq 3 depends on the dimensions and dielectric properties of the cavity and the sample and has been

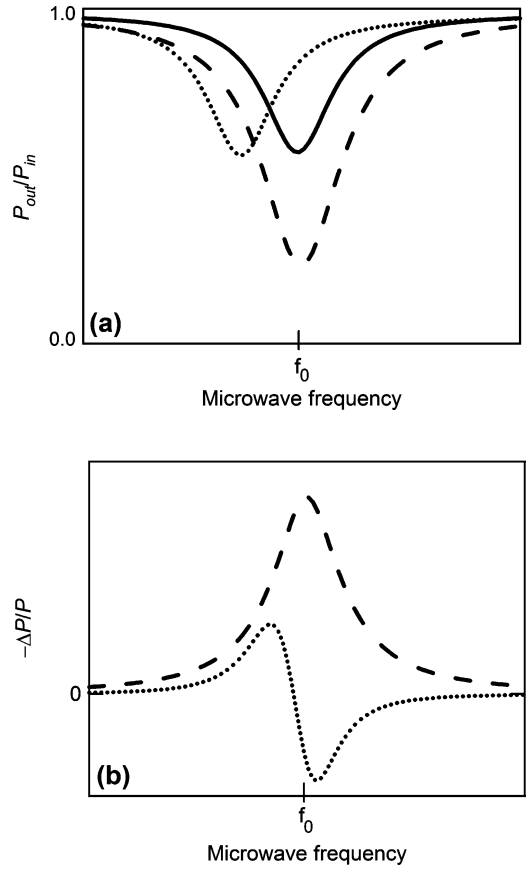

Figure 9. (a) Ratio of reflected microwave power, P_{out}, and incident power, P_{in}, *versus* microwave frequency in the absence of photoexcitation (solid line) and after a photoinduced change in only the real (dashed line) and only the imaginary (dotted line) conductance. (b) Corresponding relative change in microwave power upon photoexcitation. The resonance frequency of the cavity loaded with the sample in the absence of photoexcitation is given by f_0.

determined previously.[44] The real component of the photoconductance ΔG is[48]

$$\Delta G(t) = e\beta I_o F_a \Phi(t) \Sigma\mu \quad (4)$$

where e is the elementary charge, β is the ratio between the broad and narrow inner dimensions of the waveguide, I_o is the photon fluence in the laser pulse, F_a is the fraction of light absorbed by the sample, $\Phi(t)$ is the quantum yield of mobile charge carriers at time t per absorbed photon, and $\Sigma\mu$ is the sum of the electron and hole mobilities. After formation of mobile charge carriers by the laser pulse, the measured photoconductance increases on a time scale that is mainly determined by the 18 ns response time of the microwave cavity. The measured photoconductance reaches a maximum, ΔG_0 and subsequently decreases due to charge recombination and/or trapping at defects. The product $\Phi_0\Sigma\mu$ is obtained from ΔG_0 by use of eq 4. Since Φ_0 is less than unity, the product $\Phi_0\Sigma\mu$ corresponds to the lower limit of $\Sigma\mu$.

Acknowledgment. The authors thank R. Loef for his help with the nanocrystal synthesis, B. Cook (Faculty of Applied Sciences, Delft University of Technology) for SEM measurements, and S. Luxembourg (DIMES, Delft University of Technology) for IR transmission measurements. This work is part of SELECT-Silicon Based Superlattices with Spectrum Selective Absorbers. SELECT is financed by SenterNovem; program "Energie Onderzoek Subsidie: Lange Termijn". We further acknowledge the 3TU Centre for Sustainable Energy Technologies (Federation of the three Universities of Technology) and the Division of Chemical Sciences of NWO for VICI Award 700.53.443.

REFERENCES AND NOTES

1. Alivisatos, A. P. Perspectives on the Physical Chemistry of Semiconductor Nanocrystals. *J. Phys. Chem.* **1996**, *100*, 13226–13239.
2. Vanmaekelbergh, D.; Liljeroth, P. Electron-Conducting Quantum Dot Solids: Novel Materials Based on Colloidal Semiconductor Nanocrystals. *Chem. Soc. Rev.* **2005**, *34*, 299–312.
3. Nozik, A. J. Quantum Dot Solar Cells. *Physica E* **2002**, *14*, 115–120.
4. Kamat, P. V. Quantum Dot Solar Cells. Semiconductor Nanocrystals as Light Harvesters. *J. Phys. Chem. B* **2008**, *112*, 18737–18753.
5. Marti, A.; Araujo, G. L. Limiting Efficiencies for Photovoltaic Energy Conversion in Multigap Systems. *Sol. Energy Mater. Sol. Cells* **1996**, *43*, 203–222.
6. Schaller, R. D.; Petruska, M. A.; Klimov, V. I. Effect of Electronic Structure on Carrier Multiplication Efficiency: Comparative Study of PbSe and CdSe Nanocrystals. *Appl. Phys. Lett.* **2005**, *87*, 253102.
7. Schaller, R. D.; Klimov, V. I. High Efficiency Carrier Multiplication in PbSe Nanocrystals: Implications for Solar Energy Conversion. *Phys. Rev. Lett.* **2004**, *92*, 186601.
8. Ellingson, R. J.; Beard, M. C.; Johnson, J. C.; Yu, P. R.; Micic, O. I.; Nozik, A. J.; Shabaev, A.; Efros, A. L. Highly Efficient Multiple Exciton Generation in Colloidal PbSe and PbS Quantum Dots. *Nano Lett.* **2005**, *5*, 865–871.
9. Trinh, M. T.; Houtepen, A. J.; Schins, J. M.; Hanrath, T.; Piris, J.; Knulst, W.; Goossens, A.; Siebbeles, L. D. A. In Spite of Recent Doubts Carrier Multiplication Does Occur in PbSe Nanocrystals. *Nano Lett.* **2008**, *8*, 1713–1718.
10. Hanna, M. C.; Nozik, A. J. Solar Conversion Efficiency of Photovoltaic and Photoelectrolysis Cells with Carrier Multiplication Absorbers. *J. Appl. Phys.* **2006**, *100*, 074510.
11. Donega, C. D.; Liljeroth, P.; Vanmaekelbergh, D. Physicochemical Evaluation of the Hot-Injection Method, a Synthesis Route for Monodisperse Nanocrystals. *Small* **2005**, *1*, 1152–1162.
12. Talapin, D. V.; Rogach, A. L.; Shevchenko, E. V.; Kornowski, A.; Haase, M.; Weller, H. Dynamic Distribution of Growth Rates within the Ensembles of Colloidal II−VI and III−V Semiconductor Nanocrystals as a Factor Governing Their Photoluminescence Efficiency. *J. Am. Chem. Soc.* **2002**, *124*, 5782–5790.
13. Talapin, D. V.; Murray, C. B. Pbse Nanocrystal Solids for N- and P-Channel Thin Film Field-Effect Transistors. *Science* **2005**, *310*, 86–89.
14. Yu, D.; Wang, C.; Guyot-Sionnest, P. N-Type Conducting CdSe Nanocrystal Solids. *Science* **2003**, *300*, 1277–1280.
15. Yu, D.; Wehrenberg, B. L.; Jha, P.; Ma, J.; Guyot-Sionnest, P. Electronic Transport of N-Type CdSe Quantum Dot Films: Effect of Film Treatment. *J. Appl. Phys.* **2006**, 99.
16. Kovalenko, M. V.; Scheele, M.; Talapin, D. V. Colloidal Nanocrystals with Molecular Metal Chalcogenide Surface Ligands. *Science* **2009**, *324*, 1417–1420.
17. Talgorn, E.; Moysidou, E.; Abellon, R. D.; Savenije, T. J.; Goossens, A.; Houtepen, A. J.; Siebbeles, L. D. A. Highly Photoconductive CdSe Quantum-Dot Films: Influence of Capping Molecules and Film Preparation Procedure. *J. Phys. Chem. B* **2010**, DOI: 10.1021/jp9109546.
18. Drndic, M.; Jarosz, M. V.; Morgan, N. Y.; Kastner, M. A.; Bawendi, M. G. Transport Properties of Annealed CdSe Colloidal Nanocrystal Solids. *J. Appl. Phys.* **2002**, *92*, 7498–7503.
19. Eijt, S. W. H.; Mijnarends, P. E.; van Schaarenburg, L. C.; Houtepen, A. J.; Vanmaekelbergh, D.; Barbiellini, B.; Bansil, A. Electronic Coupling of Colloidal CdSe Nanocrystals Monitored by Thin-Film Positron-Electron Momentum Density Methods. *Appl. Phys. Lett.* **2009**, *94*, 091908.
20. Porter, V. J.; Geyer, S.; Halpert, J. E.; Kastner, M. A.; Bawendi,

M. G. Photoconduction in Annealed and Chemically Treated CdSe/ZnS Inorganic Nanocrystal Films. *J. Phys. Chem. B* **2008**, *112*, 2308–2316.
21. Peng, X. G.; Schlamp, M. C.; Kadavanich, A. V.; Alivisatos, A. P. Epitaxial Growth of Highly Luminescent CdSe/CdS Core/Shell Nanocrystals with Photostability and Electronic Accessibility. *J. Am. Chem. Soc.* **1997**, *119*, 7019–7029.
22. Kroeze, J. E.; Savenije, T. J.; Vermeulen, M. J. W.; Warman, J. M. Contactless Determination of the Photoconductivity Action Spectrum, Exciton Diffusion Length, and Charge Separation Efficiency in Polythiophene-Sensitized TiO_2 Bilayers. *J. Phys. Chem. B* **2003**, *107*, 7696–7705.
23. Peng, X. G.; Wickham, J.; Alivisatos, A. P. Kinetics of II−VI and III−V Colloidal Semiconductor Nanocrystal Growth: "Focusing" of Size Distributions. *J. Am. Chem. Soc.* **1998**, *120*, 5343–5344.
24. Murray, C. B.; Norris, D. J.; Bawendi, M. G. Synthesis and Characterization of Nearly Monodisperse CdE (E = S, Se, Te) Semiconductor Nanocrystallites. *J. Am. Chem. Soc.* **1993**, *115*, 8706.
25. Artemyev, M. V.; Woggon, U.; Jaschinski, H.; Gurinovich, L. I.; Gaponenko, S. V. Spectroscopic Study of Electronic States in an Ensemble of Close-Packed CdSe Nanocrystals. *J. Phys. Chem. B* **2000**, *104*, 11617–11621.
26. Dehaas, M. P.; Warman, J. M. Photon-Induced Molecular Charge Separation Studied by Nanosecond Time-Resolved Microwave Conductivity. *Chem. Phys.* **1982**, *73*, 35–53.
27. Yu, W. W.; Qu, L. H.; Guo, W. Z.; Peng, X. G. Experimental Determination of the Extinction Coefficient of CdTe, CdSe, and CdS Nanocrystals. *Chem. Mater.* **2003**, *15*, 2854–2860.
28. Meulenberg, R. W.; Lee, J. R. I.; Wolcott, A.; Zhang, J. Z.; Terminello, L. J.; van Buuren, T. Determination of the Exciton Binding Energy in CdSe Quantum Dots. *ACS Nano* **2009**, *3*, 325–330.
29. Ginger, D. S.; Greenham, N. C. Charge Injection and Transport in Films of CdSe Nanocrystals. *J. Appl. Phys.* **2000**, *87*, 1361–1368.
30. Brokmann, X.; Coolen, L.; Dahan, M.; Hermier, J. P. Measurement of the Radiative and Nonradiative Decay Rates of Single CdSe Nanocrystals through a Controlled Modification of Their Spontaneous Emission. *Phys. Rev. Lett.* **2004**, *93*, 107403.
31. Houtepen, A. J.; Kockmann, D.; Vanmaekelbergh, D. Reappraisal of Variable-Range Hopping in Quantum-Dot Solids. *Nano Lett.* **2008**, *8*, 3516–3520.
32. Chandler, R. E.; Houtepen, A. J.; Nelson, J.; Vanmaekelbergh, D. Electron Transport in Quantum Dot Solids: Monte Carlo Simulations of the Effects of Shell Filling, Coulomb Repulsions, and Site Disorder. *Phys. Rev. B* **2007**, *75*, 085325.
33. Razavy, M. *Quantum Theory of Tunneling*; World Scientific: River Edge, NJ, 2003.
34. Jasieniak, J.; Pacifico, J.; Signorini, R.; Chiasera, A.; Ferrari, M.; Martucci, A.; Mulvaney, P. Luminescence and Amplified Stimulated Emission in CdSe-ZnS-Nanocrystal-Doped TiO_2 and ZrO_2 Waveguides. *Adv. Funct. Mater.* **2007**, *17*, 1654–1662.
35. Houtepen, A. J.; Vanmaekelbergh, D. Orbital Occupation in Electron-Charged CdSe Quantum-Dot Solids. *J. Phys. Chem. B* **2005**, *109*, 19634–19642.
36. Berger, L. I. *Semiconductor Materials*; CRC Press: Boca Raton, FL, 1997.
37. Scholes, G. D. Insights into Excitons Confined to Nanoscale Systems: Electron−Hole Interaction, Binding Energy, and Photodissociation. *ACS Nano* **2008**, *2*, 523–537.
38. Cahen, D.; Hodes, G.; Gratzel, M.; Guillemoles, J. F.; Riess, I. Nature of Photovoltaic Action in Dye-Sensitized Solar Cells. *J. Phys. Chem. B* **2000**, *104*, 2053–2059.
39. Huijser, A.; Marek, P. L.; Savenije, T. J.; Siebbeles, L. D. A.; Scherer, T.; Hauschild, R.; Szmytkowski, J.; Kalt, H.; Hahn, H.; Balaban, T. S. Photosensitization of TiO_2 and SnO_2 by Artificial Self-Assembling Mimics of the Natural Chlorosomal Bacteriochlorophylls. *J. Phys. Chem. B* **2007**, *111*, 11726–11733.
40. Kroeze, J. E.; Koehorst, R. B. M.; Savenije, T. J. Singlet and Triplet Exciton Diffusion in a Self-Organizing Porphyrin Antenna Layer. *Adv. Funct. Mater.* **2004**, *14*, 992–998.
41. Rothenberger, G.; Fitzmaurice, D.; Gratzel, M. Spectroscopy of Conduction-Band Electrons in Transparent Metal-Oxide Semiconductor-Films—Optical Determination of the Flat-Band Potential of Colloidal Titanium-Dioxide Films. *J. Phys. Chem.* **1992**, *96*, 5983–5986.
42. Houtepen, A. J. Charge Injection and Transport in Quantum Confined and Disordered Systems. Ph.D. Thesis, Utrecht University, 2007.
43. Kucur, E.; Bucking, W.; Giernoth, R.; Nann, T. Determination of Defect States in Semiconductor Nanocrystals by Cyclic Voltammetry. *J. Phys. Chem. B* **2005**, *109*, 20355–20360.
44. Savenije, T. J.; de Haas, M. P.; Warman, J. M. The Yield and Mobility of Charge Carriers in Smooth and Nanoporous TiO_2 Films. *Z. Phys. Chem.* **1999**, *212*, 201–206.
45. Mekis, I.; Talapin, D. V.; Kornowski, A.; Haase, M.; Weller, H. One-Pot Synthesis of Highly Luminescent CdSe/CdS Core−Shell Nanocrystals *via* Organometallic and "Greener" Chemical Approaches. *J. Phys. Chem. B* **2003**, *107*, 7454–7462.
46. Kongkanand, A.; Tvrdy, K.; Takechi, K.; Kuno, M.; Kamat, P. V. Quantum Dot Solar Cells. Tuning Photoresponse through Size and Shape Control of CdSe-TiO_2 Architecture. *J. Am. Chem. Soc.* **2008**, *130*, 4007–4015.
47. Schins, J. M.; Prins, P.; Grozema, F. C.; Abellon, R. D.; de Haas, M. P.; Siebbeles, L. D. A. Development of a Microwave Transmission Setup for Time-Resolved Measurements of the Transient Complex Conductivity in Bulk Samples. *Rev. Sci. Instrum.* **2005**, *76*, 084703.
48. Kroeze, J. E.; Savenije, T. J.; Warman, J. M. Electrodeless Determination of the Trap Density, Decay Kinetics, and Charge Separation Efficiency of Dye-Sensitized Nanocrystalline TiO_2. *J. Am. Chem. Soc.* **2004**, *126*, 7608–7618.